JGR Oceans

RESEARCH ARTICLE
10.1029/2020JC016480

Key Points:

- Empirical models for estimating carbonate system parameters from basic hydrographic variables were developed for the northeast US shelf
- The best models explain over 98% of the variability in carbon variables and rely on temperature, salinity, oxygen, and nitrate
- Model equations reflect the contribution of known drivers to regional variability: biological metabolism, river input, and water mass mixing

Supporting Information:

- Figure S1

Correspondence to:
K. McGarry,
kelly.m.mcgarry@uconn.edu

Citation:
McGarry, K., Siedlecki, S. A., Salisbury, J., & Alin, S. R. (2021). Multiple linear regression models for reconstructing and exploring processes controlling the carbonate system of the northeast US from basic hydrographic data. *Journal of Geophysical Research: Oceans*, *126*, e2020JC016480. https://doi.org/10.1029/2020JC016480

Received 16 JUN 2020
Accepted 7 DEC 2020
Corrected 24 MAR 2021

This article was corrected on 24 MAR 2021. See the end of the full text for details.

Multiple Linear Regression Models for Reconstructing and Exploring Processes Controlling the Carbonate System of the Northeast US From Basic Hydrographic Data

K. McGarry[1], S. A. Siedlecki[1], J. Salisbury[2], and S. R. Alin[3]

[1]Department of Marine Sciences, University of Connecticut, Groton, CT, USA, [2]Ocean Process Analysis Laboratory, University of New Hampshire, Durham, NH, USA, [3]NOAA Pacific Marine Environmental Laboratory (PMEL), Seattle, WA, USA

Abstract In the coastal ocean, local carbonate system variability is determined by the interaction between ocean acidification and local processes. Sporadic observations indicate that biological metabolism, river input, and water mass mixing are dominant local processes driving carbonate system variability in northeast US shelf waters. These processes are also reflected in the variability of observed temperature (T), salinity (S), oxygen concentration (O_2), and nitrate concentration (NO_3^-). Therefore, regionally specific empirical models can be developed, which relate carbonate system parameters to a combination of basic hydrographic parameters. Here, we develop multiple linear regression models that represent the processes that drive carbonate system variability in the Mid-Atlantic Bight and Gulf of Maine using observations obtained on three hydrographic surveys in summers between 2007 and 2015. The empirical model equations reveal the observation-based relationships between carbonate parameters and basic hydrographic variables. Unlike other regions where empirical models have been developed, salinity appears in all models. *T* is the most important parameter for predicting aragonite saturation state (Ω_{AR}), while S and O_2 are most important for predicting pH on total scale (pH_T). The basic hydrographic variables explain over 98% of the variability in total alkalinity (TA), dissolved inorganic carbon (DIC), and Ω_{AR} and 89% of the variability in pH_T in the calibration data. We recommend applying models that depend on T, S, O_2, and NO_3^- as predictors, which reproduce TA and DIC with $R^2 > 0.97$, Ω_{AR} with $R^2 > 0.93$, and pH_T with $R^2 > 0.77$, to reconstruct carbonate system parameters in the region.

Plain Language Summary Carbon dioxide released to the atmosphere by humans can adversely impact aquatic ecosystems, so it is crucial that we understand the current state of carbon variables and anticipate future conditions. Carbon cycling in the coastal ocean is the result of the interaction of physical and biological processes that occur on multiple time and space scales. Sparse sampling of carbon variables presents challenges to our understanding of carbon cycling in the coastal ocean. Other seawater properties measured more frequently with better spatial coverage, including temperature, salinity, oxygen concentration, and nitrate concentration, can be used in combination to estimate carbon variables. In this study, we rely on measurements from cruises along the northeast US shelf to develop equations to predict carbon variables from other seawater properties. These equations can be used to fill gaps in observations and help incorporate observations into ocean models. The statistical relationships between carbon variables and other seawater properties identified here vary depending on the region, because a balance of different processes is important in each region. On the northeast US shelf, salinity emerges as an important predictor for all explored carbon variables.

1. Introduction

1.1. Purpose

In the coastal ocean, local processes can mitigate or exacerbate the effects of ocean acidification, posing a challenge to anticipating carbonate system conditions. Although prior observations in the region are limited in space and time, they have identified dominant processes driving carbonate system variability on the northeast United States (NE US) shelf, which include biological metabolism (Wallace et al., 2014; Wang

Table 1
Empirical Models Developed to Estimate Ω_{AR} in Other Regions

Citation	Region	Terms in equation
Juranek et al., 2009	Central Oregon	O_2, T·O_2
Kim et al., 2010	Sea of Japan	T, O_2, P
Alin et al., 2012	Southern California Current System	T, O_2, T·O_2
Evans et al., 2013	Northern Gulf of Alaska	S, NO_3^-

Abbreviation: Ω_{AR}, aragonite saturation state.

et al., 2017), river input (Rheuban et al., 2019; J. Salisbury et al., 2009; Wang et al., 2013), and water mass mixing (Gledhill et al., 2015; J. E. Salisbury & Jönsson 2018; Wanninkhof et al., 2015). Observational studies provide insight into the processes that control the carbonate system, but observations of the NE US shelf, which is one of the widest shelf regions in US waters, are limited in space and time. These limitations have prevented carbonate system variables from being integrated into ecosystem studies or synthesis efforts along the NE US. Downscaled biogeochemical models that address local carbonate system complexities have been developed for other regions (e.g., Laurent et al., 2017; Pilcher et al., 2019; Siedlecki et al., 2016, 2017) and for this region (Fennel, 2010; Fennel et al., 2008), but these models would benefit from the ability to incorporate more observational data, especially in the subsurface. In the carbonate system model for the NE US, dissolved inorganic carbon (DIC) and total alkalinity (TA) have been initialized using temperature- and salinity-dependent relationships derived from global observations by Lee et al. (2000) and Millero et al. (1998), but relationships derived from more recent data collected in the same region would be more ideal (Fennel, 2010; Hofmann et al., 2011). Relationships for estimating TA from salinity (S) based on recent observations have been developed by Cai et al. (2010), but their study did not explore potential predictors other than S.

In response to the sparseness of carbonate system observations, researchers have developed empirical models for estimating carbonate system parameters from basic hydrographic data in other regions (e.g., Alin et al., 2012; Evans et al., 2013; Fourrier et al., 2020; Juranek et al., 2009; Kim et al., 2010; Li et al., 2016; Table 1) as well as globally (Lee et al., 2000, 2006; Millero et al., 1998). The empirical models produced are unique to each region and depend on the balance of global and local processes controlling carbonate chemistry in each system. This approach takes advantage of more frequently observed properties that reflect the same processes affecting carbonate system variability. Estimates obtained using these empirical models supplement observations to provide a more complete picture of carbonate system variability.

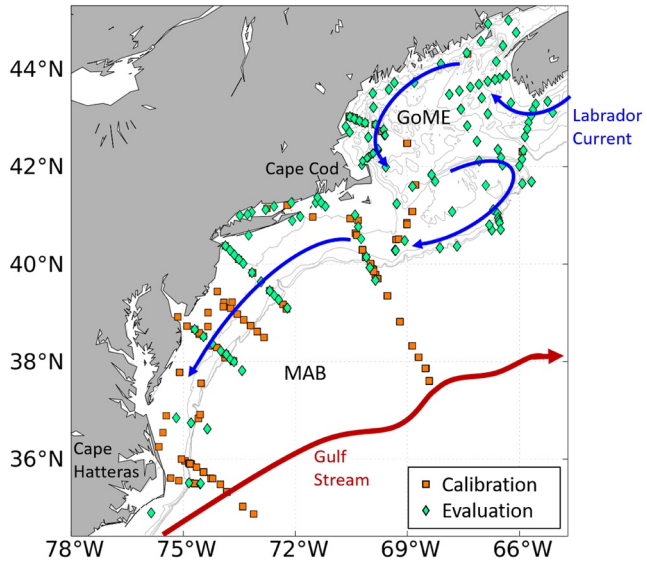

Figure 1. Observations map. Map of stations from GOMECC-1, GOMECC-2, and ECOA1 where calibration data were collected and stations from ECOA2 and repeat surveys in the southwestern Gulf of Maine where evaluation data were collected. The Gulf Stream and Labrador Current paths are shown, as well as isobaths at 50, 100, 150, and 200 m. ECOA2, East Coast Ocean Acidification 2; GOMECC, Gulf of Mexico and East Coast Carbon.

Given that these models are region-specific, here we develop a model that represents the processes that control carbonate system variability on the NE US shelf. To accomplish this, we use observations from three hydrographic surveys for calibration to develop multiparameter linear regression (MLR) models that relate each carbonate system parameter to a combination of basic hydrographic variables. The basic hydrographic variables explain nearly all the variability in carbonate parameters and the empirical models perform well in evaluation against independent data sets. The coefficients and predictors in the model equations correspond to the dominant processes controlling carbonate system variability in the region. In Section 1.2, we describe the oceanography of the study area and in Section 1.3, we summarize insights gained from past carbonate system observations in this region. We then describe the least squares multiple linear regression method that was used to develop the empirical models (2.1) as well as the methods for evaluation using an independent data set (2.2). The resulting equations (3.1) and evaluation statistics (3.2) follow. In the Discussion, we connect the MLR equations to processes controlling carbonate chemistry in the region (4.1 and 4.2), compare our model to previously developed models (4.3), discuss applications and limitations (4.4), and provide our recommendation for applying the empirical models (4.5).

1.2. Study Area

The location of this study is the NE US continental shelf, which encompasses two major subregions (Figure 1). The northeastern section is the Gulf of Maine (GoME), which extends from the Scotian Shelf to Cape

Cod. It is separated from the open North Atlantic by Georges and Browns Banks, with exchange at depths greater than 100 m limited to the Northeast Channel, through which nutrient-rich slope water can enter the GoME, driving offshore primary production (Ramp et al., 1985; Townsend 1991, 1998; Townsend et al., 2004). Southwest of Cape Cod is the Mid-Atlantic Bight (MAB), which extends to Cape Hatteras. The gently sloping MAB shelf extends more than 100 m offshore in the north and decreases to less than 30 m near Cape Hatteras (Townsend et al., 2004). Water properties throughout the NE US shelf are largely governed by influx of subpolar water from a branch of the Labrador Current which flows over the Scotian shelf, following a counterclockwise circulation in the GoME and an equatorward coastal current in the MAB (Beardsley & Winant, 1979; Chapman & Beardsley, 1989; Churchill & Berger, 1998; Csanady & Hamilton, 1988; Loder et al., 1998; Townsend et al., 2004). A shelf-break front limits exchange of the cool, fresh shelf waters with the warmer, saltier slope waters that form a buffer zone between the shelf and the Gulf Stream (Burrage & Garvine, 1988; Csanady & Hamilton, 1988; Houghton et al., 1988, 2006; Linder & Gawarkiewicz, 1998; Loder et al., 1998; Lozier & Gawarkiewicz, 2001).

1.3. Insight From Carbonate System Observations

Biological metabolism affects the carbonate system through organic matter production, which draws down DIC and nutrients in a stoichiometric ratio to oxygen (O_2) production, and remineralization, which conversely produces DIC and nutrients and draws down O_2. Calcification and dissolution of calcium carbonate also decrease and increase, respectively, TA and DIC concentrations in a 2:1 ratio. Although the shelf calcium carbonate budget is not well constrained, repeat surveys in the GoME indicate that most variability in TA and DIC on seasonal timescales is driven by photosynthesis and respiration, rather than calcification and dissolution (Wang et al., 2017).

Nearshore in the mouths of rivers, DIC production by organic matter remineralization in subsurface waters can be enhanced by nutrient loading from rivers, or eutrophication, resulting in extremely low O_2 and pH conditions in subsurface waters during summer and fall (Wallace et al., 2014). Eutrophication has contributed to corrosive conditions in estuaries and river plumes in the region (Rheuban et al., 2019; J. Salisbury et al., 2009). Rivers also influence carbonate system variability by contributing a low-alkalinity endmember (J. Salisbury et al., 2009), with TA as low as 100 μmol/kg (Wang et al., 2013). Freshwater influences carbonate chemistry on the entire shelf, but most of the freshwater is delivered by the equatorward coastal current, rather than local rivers (Cai et al., 2010; Loder et al., 1998).

Labrador Current, Gulf Stream, and slope source waters each contribute their signatures of TA and DIC to the shelf. The relative contribution of each water mass has demonstrated a trend in the recent decade (Pershing et al., 2015) and variability on shorter timescales (Gawarkiewicz et al., 2012). As low-TA Labrador current waters flow southward, accumulating DIC, this current is associated with depressed aragonite saturation state (Ω_{AR}) in the subsurface (Wanninkhof et al., 2015). The Gulf Stream endmember, with high temperature and TA, is associated with the observed Ω_{AR} increase offshore (Wanninkhof et al., 2015). Increased contribution from Gulf Stream source waters has masked the trend of ocean acidification in the GoME over the past decade (J. E. Salisbury & Jönsson 2018).

2. Methods

2.1. Calibrating Parameterizations of TA, DIC, Ω_{AR}, and pH_T in the NE US

MLR models were developed using data from three cruises along the NE US for calibration. The calibration data set ($N = 599$) includes the first and second Gulf of Mexico and East Coast Carbon (GOMECC) cruises in July–August 2007 and 2012 and the first East Coast Ocean Acidification (ECOA) cruise in June–July 2015 (Table 2). To focus on the Mid-Atlantic Bight and GoME regions, data were limited in latitude from 34.42º to 43.50º N and in longitude from 78.00º to 64.70º W, to the stations shown in Figure 1. The data were limited in depth to a minimum of 15 meters, to exclude the surface layer where air-sea gas exchange of oxygen and carbon dioxide occurs at different rates, and to a maximum depth of 500 m, to include only water masses relevant to the shelf. Observations of carbonate system parameters TA and DIC were available from every cruise. The calibration and evaluation sets of Ω_{AR} and pH_T were derived using CO2SYS version 1.1 (van Heuven et al., 2011) with the two observed carbonate parameters TA and DIC and observed T, S, silicate (Si),

Table 2
Hydrographic Surveys That Collected Calibration and Evaluation Data Used in This Study

Cruise	Start	End	*N*	Data reference
Calibration				
GOMECC 1	July 11, 2007	August 2, 2007	238	Langdon et al., 2011
GOMECC 2	July 22, 2012	August 13, 2012	257	Wanninkhof et al., 2014
ECOA 1	June 20, 2015	July 23, 2015	104	Salisbury et al., 2017
Evaluation				
ECOA 2	June 25, 2018	July 29, 2018	506	Salisbury et al., 2019
GoME	May 21, 2013	July 2, 2015	235	Wang et al., 2018

Note. *N* is the number of samples, collected at a single location, depth, and date, meeting the criteria described in Methods.

Abbreviations: ECOA, East Coast Ocean Acidification; GoME, Gulf of Mexico; GOMECC, Gulf of Mexico and East Coast Carbon.

and phosphate (PO_4) concentrations as inputs, using constants K_1 and K_2 of Lueker et al. (2000) and KSO_4 of Dickson (1990). Measurement uncertainty in TA and DIC of 2 μmol/kg (Dickson, 2010, Dickson et al., 2007) is propagated to obtain the uncertainty in pH_T and Ω_{AR} using the program of Orr et al. (2018). Only samples collected at a single location, depth, and date for which all parameters (T, S, O_2, NO_3^-, DIC, TA, Si, and PO_4) were reported and have a World Ocean Circulation Experiment (WOCE) quality control flag of 2, indicating a good value, were included in the regression.

Additional predictor variables that directly represent processes expected to affect carbonate chemistry were derived. Apparent oxygen utilization (AOU) is calculated as the difference between the O_2 concentration at saturation and the observed O_2 concentration (Weiss, 1970). Using AOU as a predictor instead of O_2 serves to isolate the change in DIC resulting from net respiration. The tracer N* is the excess NO_3^- concentration compared to the assumed ratio PO_4 produced by respiration of organic matter ($N^* = NO_3^- - 16\ PO_4$). *N** represents the combined effects of denitrification and remineralization of organic matter by N_2-fixing organisms (Sarmiento & Gruber, 2006). If there is a strong signal from aerobic respiration (AOU) or denitrification (N*) controlling carbonate system variability, then these derived predictors may appear in selected models.

The predictor parameters in the calibration set were normalized to avoid collinearity, which causes computational problems that make parameter estimates unstable (Quinn & Keough, 2002). Centering the predictor parameters by subtracting the mean of the data calibration set prevents collinearity between lower-order terms and interaction terms involving the same parameter (Quinn & Keough, 2002). The predictor data were further standardized by dividing by the standard deviation of the calibration data set, resulting in each predictor series having a mean of 0 and standard deviation of 1. Normalized predictor values are calculated using Equation 1, where X_i is the predictor variable data point, X_m is the mean of the calibration set, and X_{SD} is the standard deviation of the calibration set. This method relies on normalized predictor variables to estimate nonnormalized carbonate system variables, so the relative importance of multiple parameters can be compared within one model through the magnitude of the coefficients. However, the magnitude of coefficients between different models each predicting two different carbonate system parameters should not be compared. The normalized predictor variables were tested for collinearity by calculating the variance inflation factor (VIF) for each predictor. Combinations of terms resulting in a VIF greater than 10, indicating excessive collinearity, were rejected (Kutner et al., 2004).

$$X_n = \frac{X_i - X_m}{X_{\mathrm{SD}}} \tag{1}$$

In consideration of the abundance of observations for each predictor variable, equations with three levels of complexity are developed for predicting each carbonate system parameter. T and S are the most frequently measured parameters, so "Physical Models" were developed which depend only on T and S. For the same motivations, empirical models were developed that rely only on T, S, and O_2 ("BGC Models").

Finally, we refer to the models that include all predictors considered in this study: T, S, O_2, and NO_3 as the "BGC+ Models."

Empirical models were developed using least squares multiple linear regression of each carbonate system parameter on each combination of hydrographic variables, following the methods of Juranek et al. (2009) and Alin et al. (2012). From among the combinations allowed by VIF, each model was selected based on minimizing the Akaike Information Criterion (AIC), a metric for model selection that incorporates both the goodness of fit and a penalty for complexity (Burnham & Anderson, 2004). Using the AIC score for model selection avoids the risk of over-fitting associated with using R^2 because R^2 almost always increases when terms are added. Adding a term that reduced AIC by less than five produced negligible improvements in the accuracy of predictions, so terms reducing AIC by less than five were not added. The resulting equations are the most parsimonious models to estimate the carbonate parameters from basic hydrographic parameters. The relative AIC score (ΔAIC), the difference between each model's AIC score and the best model's AIC score, is calculated. The best overall model for estimating each carbonate system parameter is identifiable by $\Delta AIC = 0$. If adding a predictor does not improve a model, then the resulting equation is the same as the model containing fewer potential predictors (i.e., BGC + Model is the same as the BGC Model), so it is not reported. Therefore, the best model for predicting each parameter is always the reported model with the greatest number of potential predictors. The coefficient of determination (R^2) and root mean square error (RMSE) are reported as a measure of the fit of each selected model but were not relied on for model selection.

2.2. Comparison of Empirical Model Estimates to Observations From an Independent Data Set

To evaluate the ability of each selected model to predict carbonate system parameters, observed basic hydrographic parameters from independent data sets were used as inputs in the empirical models and the resulting carbonate system parameter estimates were compared to observations. The first evaluation data set ($N = 506$) was collected throughout the region during June–July 2018 (Salisbury et al., 2019). It was used to evaluate the ability of the models to predict the carbonate system during summer months, the same time of year the calibration data were collected. Model-predicted carbonate parameters were compared to the measured values of TA and DIC and CO2SYS-derived pH_T and Ω_{AR}. In addition, empirical model estimates TA_E and DIC_E were used as inputs in CO2SYS to obtain alternative estimates of pH_T and Ω_{AR} as a function of these inputs (i.e., pH_T [TA_E, DIC_E] and Ω_{AR} [TA_E, DIC_E]), which were also compared to evaluation data. The second evaluation set ($N = 235$) was collected on repeat surveys across one transect in the southwestern GoME throughout the years 2013–2015 (Wang et al., 2018). Si and PO_4 data were not available from this set so these concentrations were set to 0 in CO2SYS. Repeat GoME transects were used to evaluate the ability of the models to predict the carbonate system in seasons other than summer, when the calibration data were collected. The GoME data do not include observations of NO_3^-, so only models including T, S, and O_2 as predictor variables (BGC Models) were evaluated using this data set. Model-predicted carbonate parameters were evaluated using skill metrics R^2 and RMSE. These evaluations were the basis for developing recommendations for applying MLRs developed here.

3. Results

3.1. Resulting Parameterizations of TA, DIC, Ω_{AR}, and pH_T in the NE US

Empirical models that robustly explain the variability in the carbonate system parameters (DIC, TA, Ω_{AR}, pH_T) of the calibration set were selected. Whereas O_2 and NO_3^- were too closely related to be used together in models developed for the West Coast (Alin et al., 2012; Juranek et al., 2009), all linear combinations of hydrographic parameters tested here resulted in VIFs less than 10, suggesting that O_2 and NO_3^- are decoupled in the NE US by mixing of riverine or oceanic endmembers with different NO_3^- signatures or by denitrification. The interaction term between T and NO_3^- showed excessive collinearity with NO_3^-, so the interaction term was not included. Although derived predictors AOU and N* were tested, no model including these predictors was selected based on the AIC criteria described in Methods. Although aerobic respiration affects carbonate system variability, AOU might not have been selected as a predictor because the AOU calculation assumes the preformed concentration is equal to the saturation concentration, which may not actually be

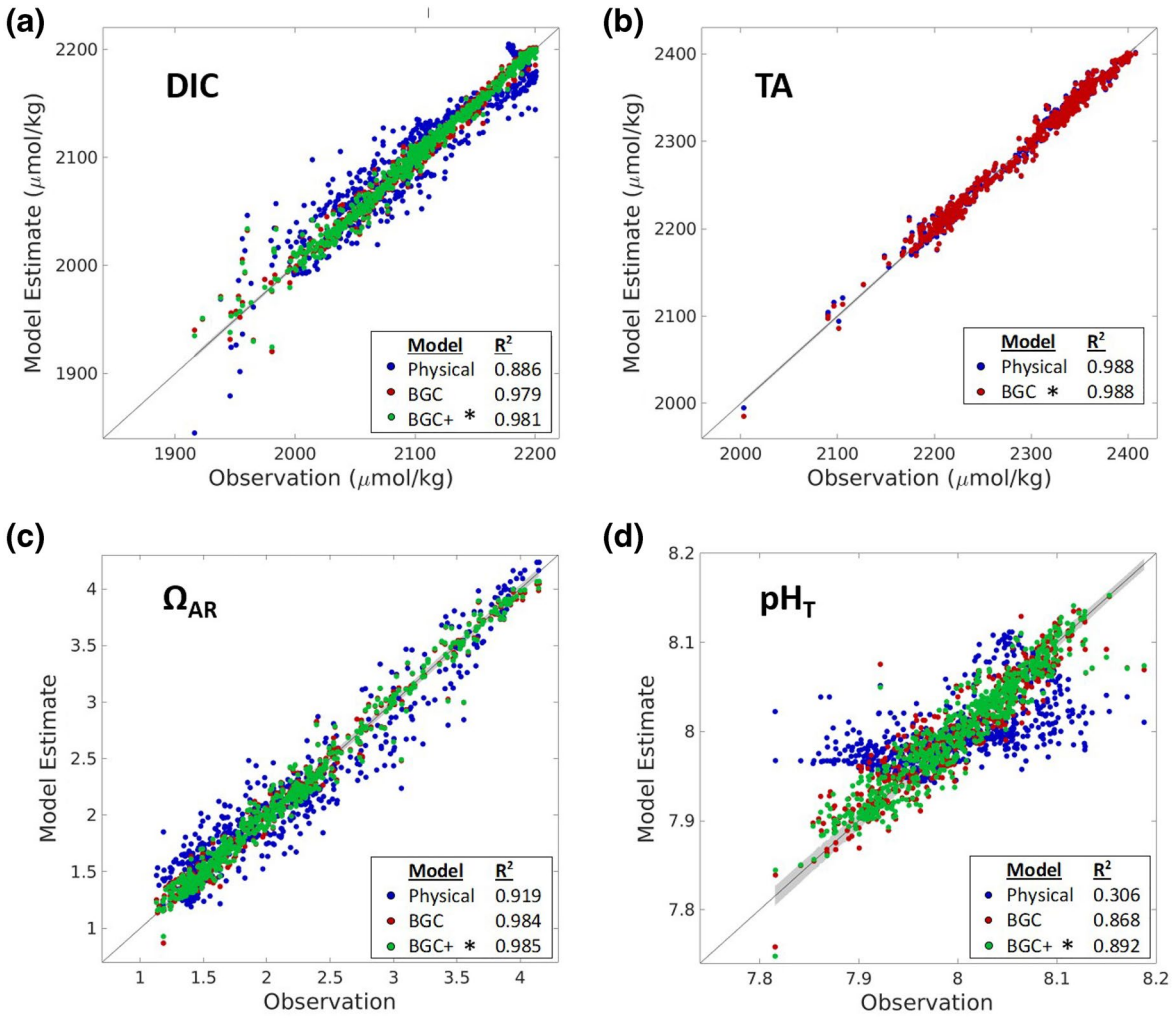

Figure 2. Empirical model calibration results. Model estimate versus observed value for calibration data for each carbonate parameter (a) DIC, (b) TA, (c) Ω_{AR}, and (d) pH on total scale (pH_T) for each combination of predictors. R^2 for each calibration fit is reported in the legend. pH_T and Ω_{AR} "observations" are derived from observed TA and DIC. 1:1 line is shown and mean measurement uncertainty (TA, DIC), and propagated uncertainty (Ω_{AR}, pH_T) is shaded. The overall best model determined by AIC score is marked with an asterisk in each panel. Ω_{AR}, aragonite saturation state; AIC, Akaike information criterion; DIC, dissolved inorganic carbon; TA, total alkalinity.

the case. Including O_2 as a predictor improved the model fit for all carbonate system parameters. Including NO_3^- resulted in improvement in the models for carbonate system variables DIC, Ω_{AR}, and pH_T, but it did not improve the model for TA, so there is no BGC + Model reported for TA. In the text that follows, selected models and calibration statistics are presented for each set of potential predictors (Table 3). The selected models for predicting each parameter are compared to inform recommendations for application. The basic hydrographic variables explain over 98% of the variability in the TA, DIC, and Ω_{AR} and 89% of the variability in pH_T in the calibration data.

With only T and S as potential predictors, the Physical Model for DIC includes all terms allowed within the constraints described in Methods: T, S, and an interaction term between T and S. Predicted DIC depends negatively on T and positively on S (Table 3). In the model including T, S, and O_2 as predictors (BGC Model), the importance of S diminishes and DIC depends negatively on O_2. Performance improves with the inclusion of O_2 (Figure 2a). In the model including T, S, O_2, and NO_3^- (BGC + Model), the coefficients of T, S, and O_2 terms are similar to those in Regression II. DIC additionally depends on NO_3^- and an interaction term between NO_3^- and S and the model performance improves slightly (Figure 2a). Of all sets of predictor variables, the best model for predicting DIC is the BGC + Model.

Table 3
Empirical Model Equations and Statistics

	No.	Form of equation	Calib. R^2	Calib. RMSE	ΔAIC	Coefficients ± standard error	Eval. R^2	Eval. RMSE
DIC	I	$\alpha_0 + \alpha_1 \cdot T_n +$ $\alpha_2 \times S_n + \alpha_3 \times T_n \times S_n$	0.886	20.8	1,060	$\alpha_0 = 2103 \pm 0.98$ $\alpha_1 = -56.4 \pm 1.1$ $\alpha_2 = 58.3 \pm 1.0$ $\alpha_3 = -7.26 \pm 0.93$	0.861	22.3
	II	$\alpha_0 + \alpha_1 \times T_n +$ $\alpha_2 \times S_n + \alpha_3 \times O_n + \alpha_4 \times T_n \times S_n$	0.979	9.0	57	$\alpha_0 = 2099 \pm 0.38$ $\alpha_1 = -52.4 \pm 0.45$ $\alpha_2 = 34.7 \pm 0.61$ $\alpha_3 = -29.7 \pm 0.58$ $\alpha_4 = -3.29 \pm 0.53$	[a]0.979 [b]0.912	[a]11.2 [b]15.5
	III	$\alpha_0 + \alpha_1 \times T_n +$ $\alpha_2 \times S_n + \alpha_3 \times O_n + \alpha_4 \times N_n +$ $\alpha_5 \times T_n \times S_n +$ $\alpha_6 \times T_n \times O_n +$ $\alpha_7 \times S_n \times N_n$	0.981	8.5	0	$\alpha_0 = 2101 \pm 0.56$ $\alpha_1 = -51.4 \pm 0.75$ $\alpha_2 = 31.3 \pm 0.73$ $\alpha_3 = -30.7 \pm 0.75$ $\alpha_4 = 1.71 \pm 0.81$ $\alpha_5 = -2.26 \pm 0.70$ $\alpha_6 = -3.88 \pm 0.70$ $\alpha_7 = -6.15 \pm 0.79$	0.978	11.7
TA	IV	$\alpha_0 + \alpha_1 \times T_n +$ $\alpha_2 \times S_n$	0.988	7.8	26	$\alpha_0 = 2289 \pm 0.32$ $\alpha_1 = 0.758 \pm 0.37$ $\alpha_2 = 69.2 \pm 0.37$	0.976	10.7
	V	$\alpha_0 + \alpha_1 \times S_n +$ $\alpha_2 \times O_n$	0.988	7.6	0	$\alpha_0 = 2289 \pm 0.31$ $\alpha_1 = 71.2 \pm 0.43$ $\alpha_2 = 2.39 \pm 0.43$	[a]0.976 [b]0.956	[a]10.9 [b]6.6
Ω_{AR}	VI	$\alpha_0 + \alpha_1 \times T_n +$ $\alpha_2 \times S_n + \alpha_3 \times T_n \times S_n$	0.919	0.214	994	$\alpha_0 = 2.065 \pm 1.0 \cdot 10^{-2}$ $\alpha_1 = 0.635 \pm 1.1 \cdot 10^{-2}$ $\alpha_2 = 6.81 \cdot 10^{-2} \pm 1.0 \cdot 10^{-2}$ $\alpha_3 = 0.101 \pm 9.6 \cdot 10^{-3}$	0.739	0.227
	VII	$\alpha_0 + \alpha_1 \times T_n +$ $\alpha_2 \times S_n + \alpha_3 \times O_n + \alpha_4 \times T_n \times S_n +$ $\alpha_5 \times T_n \times O_n$	0.984	0.095	16	$\alpha_0 = 2.11 \pm 4.7 \cdot 10^{-3}$ $\alpha_1 = 0.593 \pm 5.0 \cdot 10^{-3}$ $\alpha_2 = 0.308 \pm 6.8 \cdot 10^{-3}$ $\alpha_3 = 0.308 \pm 6.2 \cdot 10^{-3}$ $\alpha_4 = 3.36 \cdot 10^{-2} \pm 6.3 \cdot 10^{-3}$ $\alpha_5 = 5.45 \cdot 10^{-2} \pm 7.5 \cdot 10^{-3}$	[a]0.925 [b]0.606	[a]0.148 [b]0.158

Table 3
Continued

	No.	Form of equation	Calib. R^2	Calib. RMSE	ΔAIC	Coefficients ± standard error	Eval. R^2	Eval. RMSE
	VIII	$\alpha_0 + \alpha_1 \times T_n +$ $\alpha_2 \times S_n + \alpha_3 \times O_n + \alpha_4 \times T_n \times S_n +$ $\alpha_5 \times S_n \times O_n +$ $\alpha_5 \times O_n \times N_n$	0.985	0.093	0	$\alpha_0 = 2.11 \pm 5.8 \cdot 10^{-3}$ $\alpha_1 = 0.603 \pm 5.0 \cdot 10^{-3}$ $\alpha_2 = 0.308 \pm 6.8 \cdot 10^{-3}$ $\alpha_3 = 0.313 \pm 6.2 \cdot 10^{-3}$ $\alpha_4 = 2.54 \cdot 10^{-2} \pm 5.4 \cdot 10^{-3}$ $\alpha_5 = 4.05 \cdot 10^{-2} \pm 6.2 \cdot 10^{-3}$ $\alpha_6 = -4.08 \cdot 10^{-2} \pm 5.1 \cdot 10^{-3}$	0.928	0.149
pH_T	IX	$\alpha_0 + \alpha_1 \times T_n +$ $\alpha_2 \times S_n + \alpha_3 \times T_n \times S_n$	0.306	0.056	1,100	$\alpha_0 = 8.00 \pm 2.6 \cdot 10^{-3}$ $\alpha_1 = 3.59 \cdot 10^{-2} \pm 2.8 \cdot 10^{-3}$ $\alpha_2 = -5.51 \cdot 10^{-3} \pm 2.7 \cdot 10^{-3}$ $\alpha_3 = 6.84 \cdot 10^{-3} \pm 2.5 \cdot 10^{-3}$	N/A	N/A
	X	$\alpha_0 + \alpha_1 \times T_n +$ $\alpha_2 \times S_n + \alpha_3 \times O_n + \alpha_4 \times T_n \times S_n +$ $\alpha_5 \times S_n \times O_n$	0.868	0.024	112	$\alpha_0 = 8.01 \pm 1.4 \cdot 10^{-3}$ $\alpha_1 = 2.86 \cdot 10^{-2} \pm 1.3 \cdot 10^{-3}$ $\alpha_2 = 6.06 \cdot 10^{-2} \pm 1.8 \cdot 10^{-3}$ $\alpha_3 = 7.82 \cdot 10^{-2} \pm 1.6 \cdot 10^{-3}$ $\alpha_4 = -2.09 \cdot 10^{-2} \pm 1.3 \cdot 10^{-3}$ $\alpha_5 = -8.24 \cdot 10^{-3} \pm 1.4 \cdot 10^{-3}$	[a]0.778 [b]0.734	[a]0.038 [b]0.042
	XI	$\alpha_0 + \alpha_1 \times T_n +$ $\alpha_2 \times S_n + \alpha_3 \times O_n + \alpha_4 \times N_n +$ $\alpha_5 \times T_n \times S_n +$ $\alpha_6 \times S_n \times O_n +$ $\alpha_7 \times O_n \times N_n$	0.892	0.022	0	$\alpha_0 = 8.00 \pm 1.4 \cdot 10^{-3}$ $\alpha_1 = 1.20 \cdot 10^{-2} \pm 1.9 \cdot 10^{-3}$ $\alpha_2 = 6.63 \cdot 10^{-2} \pm 1.7 \cdot 10^{-3}$ $\alpha_3 = 6.51 \cdot 10^{-2} \pm 1.9 \cdot 10^{-3}$ $\alpha_4 = -2.47 \cdot 10^{-2} \pm 2.2 \cdot 10^{-3}$ $\alpha_5 = -2.04 \cdot 10^{-2} \pm 1.3 \cdot 10^{-3}$ $\alpha_6 = -9.15 \cdot 10^{-3} \pm 1.5 \cdot 10^{-3}$ $\alpha_7 = -5.03 \cdot 10^{-3} \pm 1.2 \cdot 10^{-3}$	0.810	0.035

Note. Carbonate system parameter predicted; equation number; form of each equation; R^2 and RMSE of the model estimate compared to calibration data (units of RMSE are μmol/kg for TA and DIC); ΔAIC is the difference between the AIC for each model and the best model for that parameter; R^2 and RMSE of the model estimates compared to ECOA2 evaluation data for normalizing T, S, O_2, NO_3, means ± standard deviations are 13.20 ± 5.92 °C, 34.40 ± 1.49, 214.7 ± 44.7 μmol/kg, 7.58 ± 7.65 μmol/kg.

Abbreviations: O_2, oxygen concentration; NO_3^-, nitrate concentration; pH on total scale; Ω_{AR}, aragonite saturation state; AIC, Akaike information criterion; DIC, dissolved inorganic carbon; ECOA2, East Coast Ocean Acidification 2; R^2, coefficient of determination; RMSE, root mean square error; S, salinity; T, temperature; TA, total alkalinity.

[a]Are reported for all models, R^2 and RMSE of the model estimates compared to GoME evaluation data. [b]are reported for the BGC Models.

The Physical Model for TA is a linear combination of T and S. TA is strongly correlated with S, as others have shown (e.g., Cai et al., 2010; Lee et al., 2006). Its dependence on T is weaker, with a coefficient two orders of magnitude smaller. This model explains nearly all the variability in TA (Figure 2b). In the BGC Model, O_2 replaces T in the equation, but with a slightly larger positive coefficient. The model fit improves slightly compared to the Physical Model (Figure 2b). With the addition of NO_3^- as a potential predictor, the BGC Model is still the selected model, so there is no BGC + Model reported for TA. Of the two models for predicting TA, the best is the BGC Model, which explains slightly more of the variability in TA than the Physical Model.

The Physical Model for Ω_{AR}, like that for DIC, includes all allowed terms. Ω_{AR} exhibits the strongest positive relationship with T, followed by S. In the BGC Model, the importance of the interaction term between T and S diminishes. Ω_{AR} depends strongly positively on O_2 and also on an interaction term between T and O_2 (Figure 2c). The model explains 98.4% of the variability in Ω_{AR}, compared to 91.9% for the Physical Model. In the BGC + Model, NO_3^- appears only in an interaction term with O_2. The fit improves slightly ($R^2 = 0.985$), in comparison to the BGC Model (Figure 2c). The overall best model for predicting Ω_{AR} is the BGC + Model. The fit of the BGC and BGC + Models are similar, with a difference of only 0.001 in R^2 and a difference in AIC of 15 points.

Finally, the Physical Model for pH_T includes all allowed terms: T, S, and an interaction term between T and S. The model does not fit the data well, as demonstrated by R^2 of 0.306. (Figure 2d). In the BGC Model, pH_T exhibits the strongest relationship with O_2 compared to other predictors. It also depends weakly on an interaction term between O_2 and S. The fit improves with the inclusion of O_2 ($R^2 = 0.868$, Figure 2d). In the BGC + Model, the importance of T and O_2 terms diminish, and pH_T depends negatively on NO_3^- and an interaction term between O_2 and NO_3^-. The model fit improves ($R^2 = 0.892$, Figure 2d). The best model for predicting pH_T is the BGC + Model.

3.2. Results of Comparison of Empirical Model Estimates to Independent Data Set

In general, evaluation performance using ECOA2 summer observations (Table 3) follows the trends observed from the calibration results: model estimates that fit the calibration data well also perform well in evaluation. The most complex empirical models perform well in evaluation against ECOA2 data, estimating TA and DIC with $R^2 > 0.97$, Ω_{AR} with $R^2 > 0.92$, and pH_T with $R^2 > 0.81$. The BGC Models were also evaluated against seasonal observations (Table 3). All models predict ECOA2 data with better performance than they predict GoME data, based on R^2, but error in the GoME estimates does not correlate with the time of year (Figure 4a), suggesting the MLRs can be applied in all seasons.

The Physical Model for DIC performs well against observations, with an R^2 value near the calibration value. However, at the highest DIC values (above ~2,160 μmol/kg), model estimates do not follow observations (Figure 3a.). The error at high DIC is corrected in the BGC Model. The performance of the BGC + Model is similar. The BGC Model performs worse when evaluated using GoME data, but still performs well.

The Physical Model for TA performs well against ECOA2 observations (Figure 3b). Performance of the BGC Model is nearly equal. This model also performs well when evaluated against the GoME data set (Figure 4b).

The Physical Model for Ω_{AR} tends to overestimate low values of Ω_{AR} (close to 1) by as much as 1 unit, and underestimate higher values over 2 (Figure 3c). The BGC Model performs much better than the Physical Model. The BGC + Model performance is nearly equal, with slightly greater R^2, but also greater RMSE. There are some samples for which NO_3^- is important, corresponding to shallow bottom depths and relatively low O_2. The BGC Model performance declines but still adequately represents the observations when evaluated against GoME data (Figure 4c). Using the overall best models for TA and DIC as inputs, Ω_{AR} (TA_E, DIC_E) evaluated using ECOA2 performs slightly better than the BGC + Model (Figure 3e).

The Physical Model for pH_T did not achieve a good fit with calibration data, so this model was not evaluated. In evaluation using ECOA2 data, the BGC Model performs well, and the BGC + Model performs better. The BGC Model performs similarly in evaluation using GoME data (Figure 4d). Using the overall best models for TA and DIC as inputs, pH_T (TA_E, DIC_E) evaluated using ECOA2 performs worse than the BGC + Model (Table 4, Figure 3f).

Table 4
Evaluation of Alternative pH_T and Ω_{AR} Estimates From Empirical Model TA and DIC

Carbon variable	Predictors	R^2 (direct empirical)	R^2 (TA_E, DIC_E)	RMSE (TA_E, DIC_E)
Ω_{AR}	T, S	0.739	0.752	0.221
	T, S, O_2	0.925	0.927	0.147
	T, S, O_2, NO_3^-	0.928	0.934	0.149
pH_T	T, S	N/A	0.147	0.065
	T, S, O_2	0.778	0.749	0.041
	T, S, O_2, NO_3^-	0.810	0.772	0.042

Note. Predictors used for each estimate; R^2 of carbonate system estimates directly from empirical models evaluated using ECOA2 observations; R^2 of the parameter derived from TA and DIC empirical model estimates (TA_E, DIC_E, respectively) as inputs in CO2SYS; RMSE of parameters derived from TA and DIC estimates.

Abbreviations: pH on total scale; Ω_{AR}, aragonite saturation state; AIC, Akaike information criterion; DIC, dissolved inorganic carbon; ECOA2, East Coast Ocean Acidification 2; R^2, coefficient of determination; RMSE, root mean square error; S, salinity; T, temperature; TA, total alkalinity.

4. Discussion

Empirical model equations developed here reveal the observation-based, quantitative relationships between carbonate parameters and basic hydrographic variables. The equations themselves reveal varying levels of complexity necessary to reproduce the variability in different carbonate variables and highlight regional processes that are vital to representing the carbonate system in the NE US. In the discussion, the details of the equations and their implications for processes in the region are explored and potential applications are presented.

4.1. Importance of Biological Predictor Variables

Different carbon variables require varying degrees of complexity of predictors, consistent with our understanding of the regional drivers of their variability. The simplest models presented, the Physical Models, explain nearly all the variability in TA ($R^2 = 0.988$, RMSE = 7.8 μmol/kg). TA is strongly correlated with S throughout the ocean because TA is mainly controlled by input and evaporation of freshwater and thus S has been used to predict surface TA globally (Lee et al., 2006; Millero et al., 1998). The BGC Model fits the TA calibration data slightly better, with the same R^2 and slightly reduced RMSE compared to the Physical Model. The correlation between TA and O_2 could reflect conservative mixing of end-members with different TA and O_2, but it may also reflect TA generation on the shelf by metabolic processes. The uptake of NO_3^- and ammonium in primary production is accompanied by an increase and decrease in alkalinity, respectively (Brewer & Goldman 1976; Goldman & Brewer 1980). Overall, these alkalinity changes are balanced by ammonium and NO_3^- production by organic matter decomposition, but if these processes are spatially decoupled in the water column, they can influence local alkalinity (Chen, 2002). The best model for predicting TA, Regression V, includes a positive relationship between O_2 and TA, which corresponds to TA consumption accompanying O_2 consumption by organic matter respiration. In a recent analysis of the processes controlling carbonate chemistry along US coasts, the correlation between TA and O_2 was significant only on the Atlantic coast, but not the Pacific or Gulf Coasts (Cai et al., 2020, supporting information). This is consistent with the selection of O_2 in our TA model, whereas O_2 is not used as a predictor for TA on the Pacific Coast (Alin et al., 2012; Evans et al., 2013).

Including O_2 improved the TA model, but it was even more necessary as a predictor for the other carbonate system variables DIC, Ω_{AR}, and pH_T. The residuals in the calibration data for the Physical Models for estimating all these variables were significantly correlated with O_2. The Physical Model underestimates DIC in low O_2 conditions and overestimates DIC in high O_2 conditions. O_2 was selected in every model in which it was included as a potential predictor, which highlights the importance of biological processes in controlling carbonate chemistry in the region. O_2 is linked to the carbonate system primarily due to O_2 and CO_2 appearing on opposite sides of the primary production and respiration reactions. For the typical expression of these reactions involving organic matter containing 106 moles of carbon, the widely-used ratios reported by Redfield et al. (1963) include a stoichiometric coefficient of 138 for oxygen, corresponding to a ΔO_2:ΔDIC ratio of 1.3. However, more recent studies have reported a range of values (Anderson & Sarmiento, 1994; Martin et al., 1987; Peng & Broecker, 1987; Takahashi et al., 1985; Thomas, 2002). The coefficient for oxygen in the empirical model developed here corresponds to a ΔO_2:ΔDIC ratio of 1.5. This ratio matches closely with the result found by Takahashi et al., (1985) for the North Atlantic, of ΔO_2: ΔDIC ratio of 1.54, before adjusting for water mass mixing. With O_2 as an indicator for organic matter synthesis and respiration, models reported here explain over 98% of the variability in DIC and Ω_{AR} and 89% of the variability in pH_T.

Adding NO_3^- as a predictor in the models for DIC and Ω_{AR} (BGC + Models) did not improve overall performance in the DIC model and improved performance slightly for the Ω_{AR} model (Table 3). This is not surprising because NO_3^- and O_2 provide generally the same information. Both are involved in the most common biological reactions: photosynthesis and aerobic respiration. However, including NO_3^- improved estimates

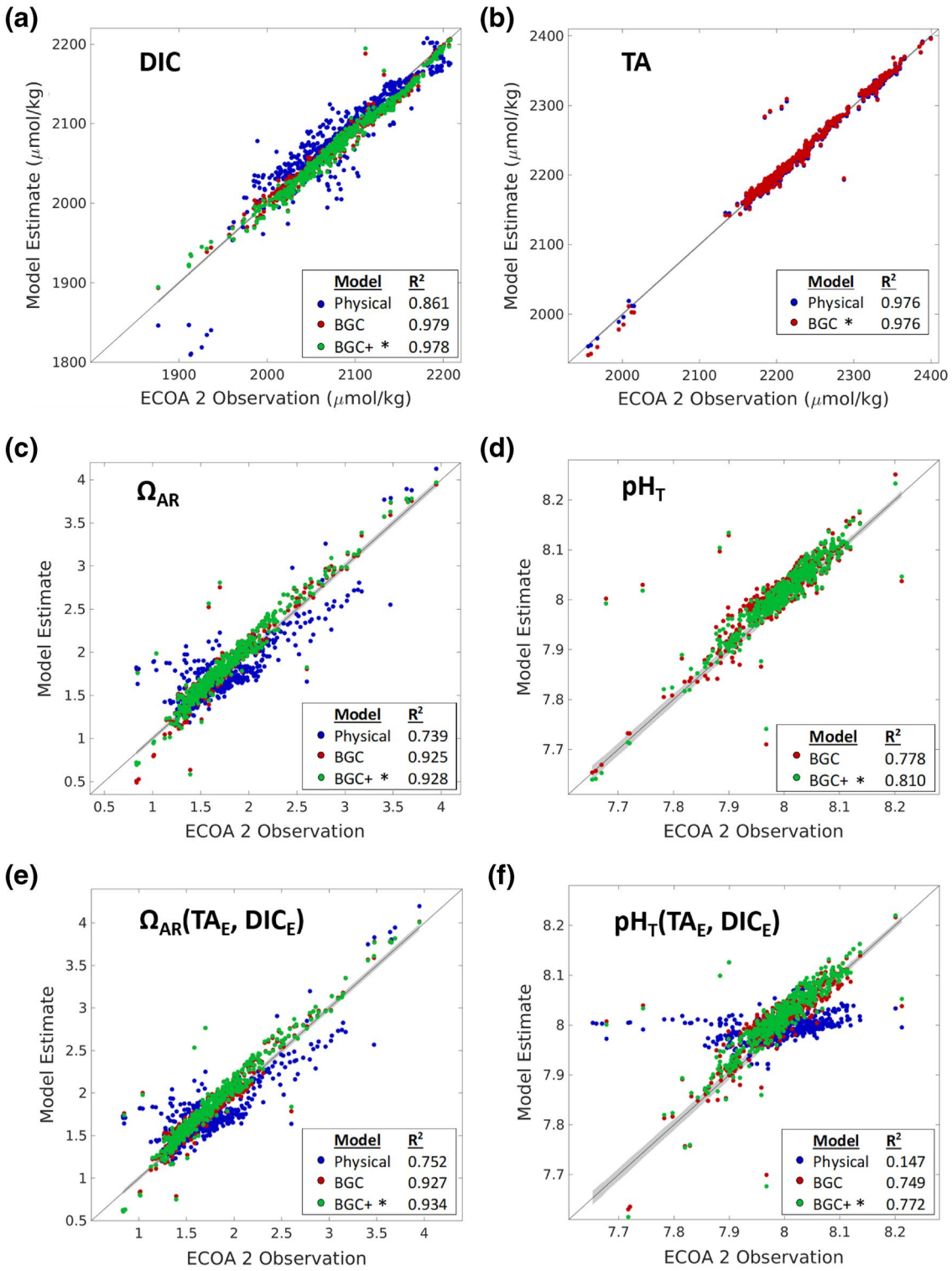

Figure 3. Empirical model evaluation results.Model estimate versus observed value for evaluation using the ECOA2 data set, which was not used for calibration, for (a) DIC, (b) TA, (c) Ω_{AR}, and (d) pH on total scale (pH_T). Panels (e and f) show the estimates obtained using empirical model estimates for TA and DIC as inputs in CO2SYS to derive pH_T (TA_E, DIC_E) and Ω_{AR}(TA_E, DIC_E). pH_T and Ω_{AR} "observations" are derived from observed TA and DIC. 1:1 line is shown and mean measurement uncertainty (TA, DIC), and propagated uncertainty (Ω_{AR}, pH_T) is shaded. The overall best model determined by AIC score is marked with an asterisk in each panel. Ω_{AR}, aragonite saturation state; AIC, Akaike information criterion; DIC, dissolved inorganic carbon; ECOA2, East Coast Ocean Acidification 2; TA, total alkalinity.

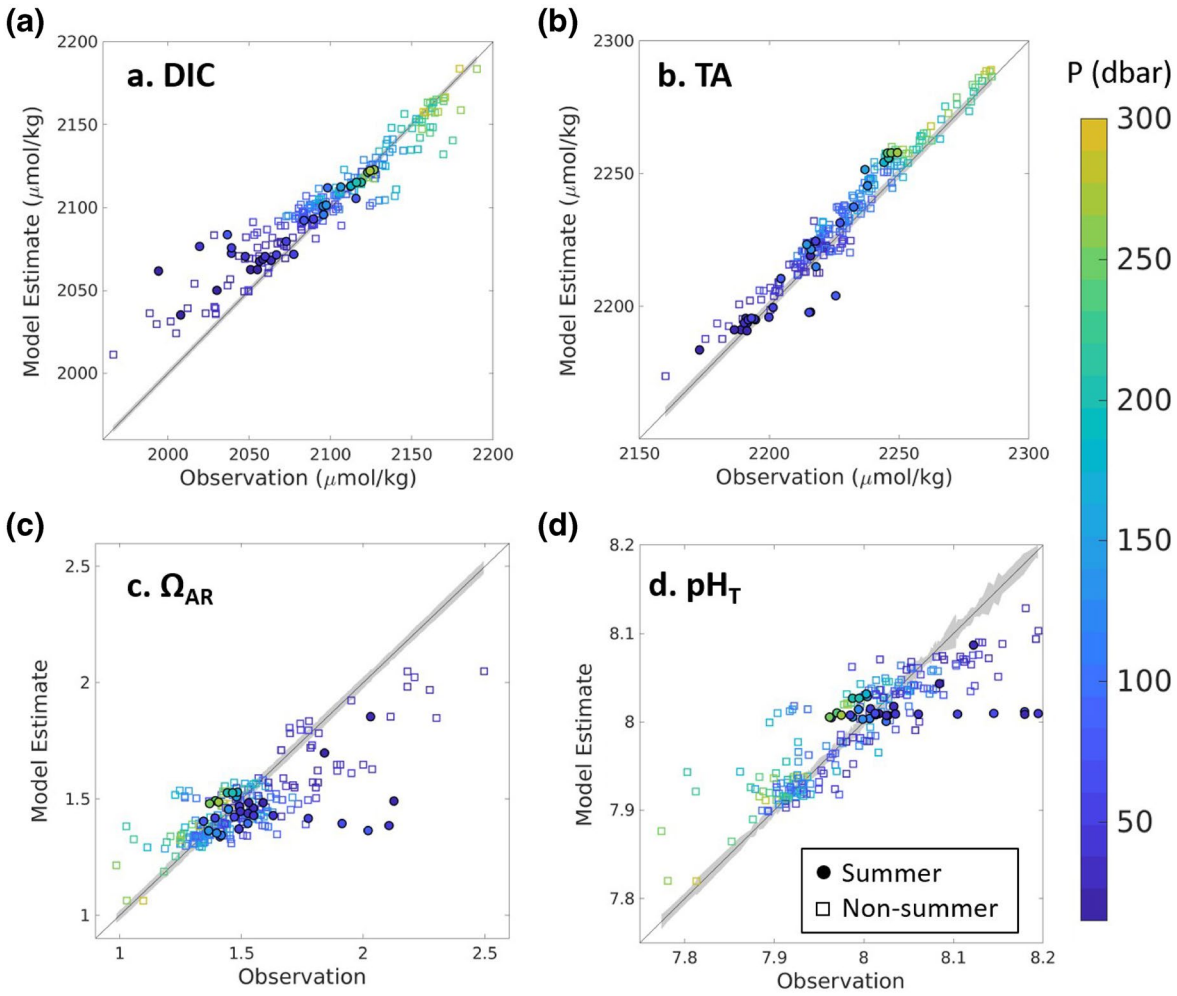

Figure 4. Evaluation of BGC empirical models using observations collected on repeat surveys of the Gulf of Maine for (a) DIC, (b) TA, (c) Ω_{AR}, and (d) pH on total scale (pH_T). "Summer" data, shown by filled circles, were collected during the time of year when the calibration data were collected, between June and August, and "Non-summer" data, shown by open squares, were collected during other times of year. Points are colored by observed pressure in decibar. pH on total scale (pH_T) and Ω_{AR} "Observations" are derived from observed TA and DIC. 1:1 line is shown and mean measurement uncertainty (TA, DIC), and propagated uncertainty (Ω_{AR}, pH_T) is shaded. DIC, dissolved inorganic carbon; TA, total alkalinity.

in some areas. The ECOA2 evaluation data set included more observations within Long Island Sound than calibration data. Though data were limited, this allowed us to explore model performance in estuarine environments. Although the BGC Model was sufficient to provide a good estimate of most DIC and Ω_{AR} data, the BGC + Model improved estimates in Long Island Sound (Figure 5), suggesting that NO_3^- might be a more important predictor of carbonate system variability in estuarine environments.

4.2. Model Equations Reflect Drivers of Carbonate System Variability Specific to NE US

Even when all four basic hydrographic parameters are available as predictor variables (BGC + Models), salinity is included in every model. This is unlike the models developed for the California Current System (CCS), because each model uniquely reflects the processes driving carbonate system variability in the region for which it was calibrated. Whereas empirical models for the CCS reflect the impact of seasonal upwelling of cold waters rich in nutrients and DIC (Alin et al., 2012; Cai et al., 2020), empirical models developed here reflect the importance of freshwater input and regional water mass variability in driving carbonate system variability. We demonstrate the necessity for region-specific models by applying the CCS empirical model to data collected in the NE US. Although this model performs well using data for the CCS region (Alin

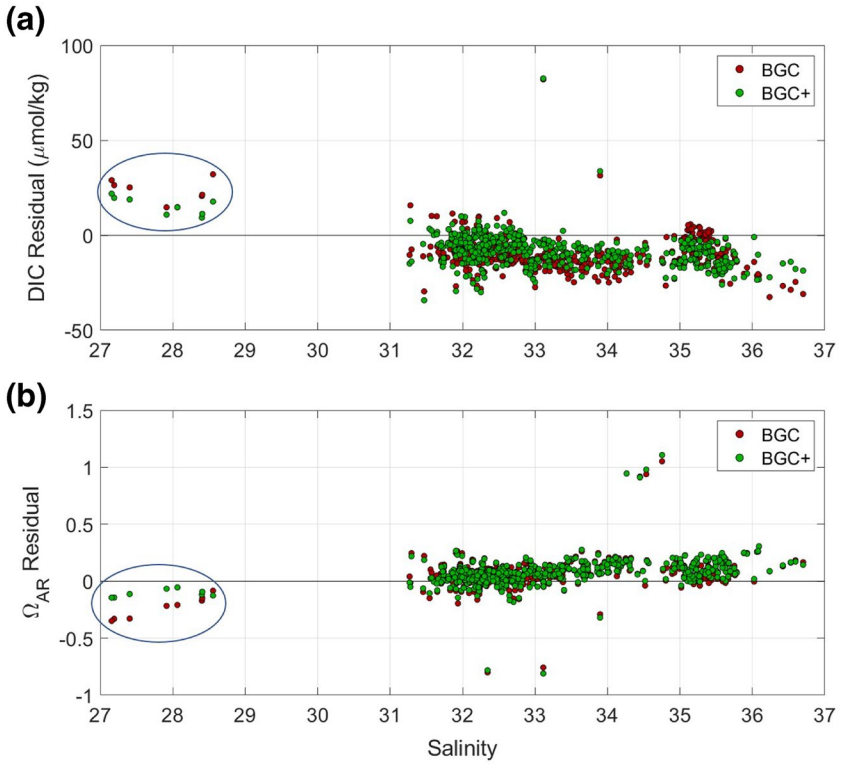

Figure 5. Residuals of DIC and Ω_{AR} vs. salinity for ECOA2 evaluation. Comparison of residuals (estimate _ observed) for of DIC and ΩAR using BGC and BGC + Models. Data points within Long Island Sound ($N = 8$) are circled in blue. Ω_{AR}, aragonite saturation state; DIC, dissolved inorganic carbon; ECOA2, East Coast Ocean Acidification 2.

et al., 2012), it is not suitable for predicting Ω_{AR} in the NE US (Figure 6). As the model equations developed here for Ω_{AR} show, the net effect of increased freshwater delivery in this region is to depress Ω_{AR}. All empirical model equations developed here to estimate DIC, Ω_{AR}, and pH_T also include an interaction term between T and S (Table 3), which corresponds to the contrast between warm, salty Gulf Stream water and cool, fresh Labrador Current water.

In recent years, the variable contribution of Gulf Stream and Labrador Current endmembers has played an important role in driving the trend in carbonate system variables in the region. Between 2004 and 2013, a northward shift in the Gulf Stream position, which reduced the southward transport of cold waters, caused the GoME to warm faster than 99.9% of the global ocean (Pershing et al., 2015). Warming impacts the carbonate system through two main processes: chemical speciation of DIC and air-sea gas exchange. The two effects nearly cancel for pH_T, but they reinforce each other for Ω_{AR}, so that warming leads to increased Ω_{AR} (Cai et al., 2020; Jiang et al., 2019). Because of this, thermodynamic forcing led to an increasing trend in Ω_{AR}, but not pH_T, during the period of intense warming (J. E. Salisbury & Jönsson 2018). This also explains why T is the most important parameter for predicting Ω_{AR}, while S and O_2 are the most important for predicting pH_T. This is consistent with models developed for the southern CCS, in which T is the most important parameter for predicting Ω_{AR} and O_2 is the most important parameter for predicting pH_T (Alin et al., 2012).

High freshwater input in the NE US was expected to present a challenge to fitting empirical models, due to the difference in chemical signature among rivers (Alin et al., 2012). However, empirical models developed here for the NE US achieve a similarly good fit to those developed for the CCS. The only parameter that did not have a similarly good fit was pH_T. Our best empirical model explained 89% of the variability in pH_T, while the CCS model explained 98% (Alin et al., 2012). One source of error in the models for estimating pH_T is our use of the TA-DIC pair to estimate pH_T, which adversely affects precision and introduces potential for adverse impacts on accuracy (Patsavas 2015; Takeshita et al., 2020). It results in a greater uncertainty in pH_T estimates compared with Ω_{AR}, as the shaded areas in Figures 2–4 reflect. Although the R^2 obtained by our model is lower than Alin et al.'s (2012), our RMSE (0.024) is equal. Furthermore, the lower perfor-

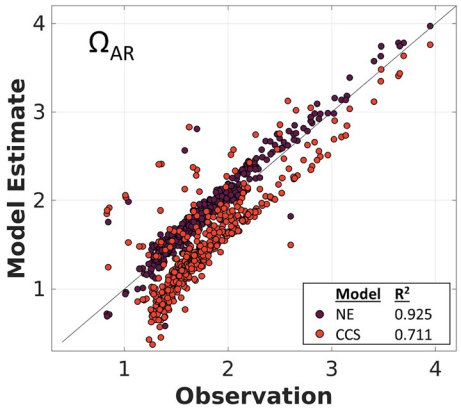

Figure 6. Aragonite saturation state estimated using a model calibrated for the California Current System and the best empirical model calibrated for the NE US. We applied Alin et al.'s (2012) model for estimating aragonite saturation state in the California Current System to the ECOA2 evaluation data. We compared the performance in the NE US to Regression VIII, developed here. NE US, Northeast United states.

mance of the pH_T model compared to other carbonate parameters is consistent with an empirical model developed for predicting surface carbonate system conditions the MAB, which resulted in R^2 values of 0.96 for DIC, 0.94 for Ω_{AR}, and 0.83 for pH_T (Xu et al., 2020). The alternative method applied here to estimate pH_T, which uses empirical model estimates for TA and DIC as inputs in CO2SYS to calculate pH_T (TA_E, DIC_E), did not improve evaluation, which makes sense because error in the pH_T calculation also affects the evaluation observations (Figure 3f).

4.3. Comparison Between Empirical Models Developed Here and Previously Developed Models

We compared our best empirical model for TA to those developed in Cai et al. (2010), which depend only on S and include five different equations for subregions and salinity ranges throughout the NE US. The single equation developed here (Regression V), which includes O_2 in addition to S, applied across a wide range of salinity environments (27–37) performs similarly to the empirical relationships of Cai et al. (2010). While the MLR developed here represents a larger fraction of the variability in TA than Cai et al. (2010) models for the Woods Hole Transect and GoME, the Cai et al. model, as well as the updated relationship reported in Xu et al. (2020), represent a larger fraction of variability in the MAB (Figure 7). This comparison indicates that including O_2 as a predictor enables our MLR to represent TA in the entire region across the full range of salinities, as opposed to requiring a stepwise function.

We have shown above that regression models developed for use in a specific region cannot be applied to a different region (Figure 6). An alternative method for estimating carbonate system parameters is available in the CANYON neural network-based approach, which provides estimates of TA, DIC, and pH_T and partial pressure of CO_2, as well as nutrient concentrations, using inputs of T, S, and O_2 as well as latitude, longitude, depth, and date (Sauzede et al., 2017). We applied this algorithm to our evaluation data. The CANYON model reproduces ECOA2 DIC, TA, and pH_T well (Figure S1), but errors in the estimates increased with decreasing salinity. Though this model works well, it may not be ideal for nearshore areas. Overall, MLR models developed here performed similarly for DIC and TA, but better for pH_T. Although it may be possible to estimate carbonate system parameters across a range of environments using one neural-network based model, the regional empirical model provides additional value because it provides the relationships between variables, which can be used to learn about the processes controlling carbonate system variability.

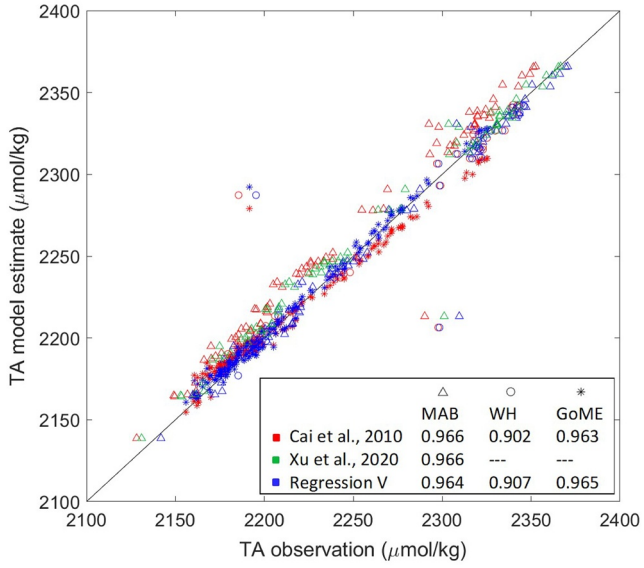

Figure 7. Comparison of salinity-TA relationships evaluated using ECOA2 data. Relationships for estimating TA from S reported in Cai et al. (2010) as five separate equations for three subsections of the region and two salinity ranges applied to ECOA2 salinity data and plotted against ECOA2 TA observations. An updated relationship reported in Xu et al. (2020) for the MAB is also compared. ECOA2, East Coast Ocean Acidification 2; TA, total alkalinity.

4.4. Applications and Limitations

Empirical models for TA, DIC, and Ω_{AR} fit the data well, explaining over 98% of the variability in each, and perform well when tested against an independent observation set. Therefore, they can be applied to T, S, O_2, and NO_3^- data to obtain robust estimates of the carbonate system parameters where carbonate system data are not available. Some examples of these applications are discussed below.

4.4.1. Seasonal Reconstruction

Most carbonate system observations are recorded during summer months. Thus, there is strong motivation to apply the empirical models to year-round basic hydrographic data to reconstruct the seasonal cycle of carbonate chemistry, as has been done in other regions (Davis et al., 2018). However, the models themselves were calibrated using only summer data. The overall performance of the model decreased when it was evaluated against a seasonal data set collected in

the GoME, but the error in these seasonal estimates was not greater outside of the season for which the models were calibrated, so the error cannot be attributed to seasonality. Instead, the reduction in performance seems to be related to processes near the surface that are important in this region that the model does not capture (Figure 4). It is possible that the BGC+ Model would account for these processes, but this cannot be confirmed because NO_3^- was not measured in the GoME data set. Because the error in the GoME estimates does not correlate with the time of year they were collected, the results suggest that the models can be applied to year-round data.

4.4.2. Historical Reconstruction and Future Projection

As concern about ocean acidification has grown, most carbonate system observations have been collected in recent years. The GOMECC-1 survey in 2007 was the first to collect comprehensive measurements of inorganic carbonate system parameters throughout the NE US (Wang et al., 2013). Thus, there is motivation to apply empirical models to historical basic hydrographic data to reconstruct past carbonate system parameters. Furthermore, there is motivation to apply the empirical models to future projections of ocean physics to anticipate the carbonate system conditions that will occur as ocean acidification progresses. However, these empirical models do not account for anthropogenic addition of CO_2, which changes the ratio of CO_2:O_2. Following the analysis of Juranek et al. (2011) comparing model error to the trends in pH and Ω_{AR}, we also estimate that it would take approximately 10 years for the error due to anthropogenic emissions to exceed the model uncertainty. Outside of this period, DIC estimates can be adjusted to account for the anthropogenic CO_2 addition. This requires determining the amount of anthropogenic CO_2 that has accumulated between the estimation period and the MLR calibration period. The ΔC^* method can be used to calculate the anthropogenic CO_2 invasion, but this method requires CFC measurements (Gruber et al., 1996). Although it was not possible to apply the ΔC^* method to their data set, Kim et al. (2010) adjusted their empirical model estimates of DIC in the Sea of Japan using estimates of anthropogenic CO_2 invasion for the Sea of Japan obtained through a different study. As Alin et al. (2012) point out, these estimates will not account for potential feedbacks such as ocean circulation associated with warming. As longer time series of carbonate system observations become available, the validity of these adjustments can be evaluated.

4.4.3. Dynamic Modeling

Finally, these empirical models can be used to improve dynamic models of the carbonate system. Though downscaled models including the carbonate system exist for this region, they would benefit from a better ability to incorporate observations (Fennel, 2010). The empirical model equations presented in this study demonstrate the observation-based relationships between carbonate system parameters and other water properties. Relationships between modeled variables can be compared to these empirical relationships to identify important processes that are not represented well in dynamic models. Furthermore, we can use the empirical models to generate initial and boundary conditions from global model data that either do not include carbonate chemistry or do not represent it well in this region. In this way, these empirical models contribute to progress toward a dynamic model that improves understanding and enables future projections of carbonate chemistry in the region.

4.5. Recommendation

We recommend applying the models of the highest complexity (Equations III, V) to existing T, S, O_2, and NO_3^- data to generate estimates of TA and DIC as these models were selected as the best when all parameters were included. If NO_3^- data are not available, models including T, S, and O_2 (Equations II, IV) are sufficient to predict carbonate parameters in most environments, but may lead to errors in estuaries and embayments. Two different methods have been presented for estimating Ω_{AR} and pH_T: direct estimate using the pH_T and Ω_{AR} empirical model equations and indirect estimate using empirical model TA and DIC as inputs in CO2sys (pH_T [TA_E, DIC_E], Ω_{AR} [TA_E, DIC_E]). Of these options, we recommend the pH_T (TA_E, DIC_E) and Ω_{AR} (TA_E, DIC_E) method. This recommendation is supported by the Ω_{AR} evaluation results: Ω_{AR} (TA_E, DIC_E) performed better in evaluation than the direct Ω_{AR} equation (Table 4). Although the direct pH_T equation performed better in evaluation, we still recommend pH_T (TA_E, DIC_E) as the best practice because the empirical models for pH_T and Ω_{AR} were calibrated using data derived from TA and DIC measurements in CO2sys, so any error resulting from that calculation is embedded in the empirical model. Another reason

we recommend the pH_T (TA_E, DIC_E) and Ω_{AR} (TA_E, DIC_E) approach is because the intermediate calculation of DIC is necessary for adding or subtracting the anthropogenic contribution if the models are applied outside of the calibration time period. Although we favor the approach using only the TA and DIC empirical model equations, we still find it useful to report the pH_T and Ω_{AR} empirical model equations to explore the processes driving variability in those parameters.

5. Conclusion

Through application of an MLR approach, we have developed empirical models for estimating carbonate system parameters TA, DIC, Ω_{AR}, and pH_T from basic hydrographic variables. This method has been applied in other regions, but the empirical model equations developed here uniquely reflect the processes that drive carbonate system variability on the NE US shelf. Salinity was selected as a predictor in all models, reflecting the importance of freshwater input. O_2 was also selected in all models where it was a potential predictor, reflecting the influence of biological metabolism. The basic hydrographic variables explain over 98% of the variability in the TA, DIC, and Ω_{AR} and 89% of the variability in pH_T in the calibration data. The recommended models perform well in evaluation against an independent data set not used in calibration, estimating TA and DIC with $R^2 > 0.97$, Ω_{AR} with $R^2 > 0.93$, and pH_T with $R^2 > 0.77$. The equations reveal observation-based relationships between carbonate parameters and basic hydrographic variables unique to the NE US shelf that build upon prior knowledge in the region. Empirical model estimates can supplement carbonate system observations to provide a better understanding of the variability of the system in space and time or be used to create boundary conditions in dynamic regional models.

Data Availability Statement

Discrete bottle data from all NOAA ocean acidification regional research cruises are available from NOAA's National Centers for Environmental Information. For GOMECC-1, [https://data.nodc.noaa.gov/cgi-bin/iso?id=gov.noaa.nodc:0066603]; for GOMECC-2, [https://data.nodc.noaa.gov/cgi-bin/iso?id=gov.noaa.nodc:0117971] or [https://doi.org/10.7289/v5542kj0]; For ECOA1, [https://www.nodc.noaa.gov/oads/data/0159428.xml] or [https://doi.org/10.7289/v5vt1q40]; for GoME repeat cruises, [https://data.nodc.noaa.gov/cgi-bin/iso?id=gov.noaa.nodc:0172591] or [https://doi.org/10.7289/v5765cn]; and for ECOA2, [https://data.nodc.noaa.gov/cgi-bin/iso?id=gov.noaa.nodc:0196419] or [https://doi.org/10.25921/f4vg-g356]

Acknowledgments
This work was partially supported by NOAA OAP (NA19OAR0170351) and The National Center for Atmospheric Research, which is a major facility sponsored by the National Science Foundation under Cooperative Agreement No. 1852977. We would like to thank Matt Long and Emily Norton for helpful discussions. SRA was funded by NOAA/PMEL, the NOAA Ocean Acidification Program, and the former NOAA Global Carbon Cycle Program. This is PMEL contribution number 5099.

References

Alin, S. R., Feely, R. A., Dickson, A. G., Hernández-Ayón, J. M., Juranek, L. W., Ohman, M. D., & Goericke, R. (2012). Robust empirical relationships for estimating the carbonate system in the southern California Current System and application to CalCOFI hydrographic cruise data (2005-2011). *Journal of Geophysical Research*, *117*, C05033. https://doi.org/10.1029/2011JC007511

Anderson, L. A., & Sarmiento, J. L. (1994). Redfield ratios of remineralization determined by nutrient data analysis. *Global Biogeochemical Cycles*. *8*(1), 65–80. https://doi.org/10.1029/93GB03318

Beardsley, R. C., & Winant, C. D. (1979). On the mean circulation in the Mid-Atlantic Bight. *Journal of Physical Oceanography*. *9*(3), 612–619. https://doi.org/10.1175/1520-0485(1979)009<0612:otmcit>2.0.co;2

Brewer, P. G., & Goldman, J. C. (1976). Alkalinity changes generated by phytoplankton growth1. *Limnology and Oceanography*, *21*(1), 108–117. https://doi.org/10.4319/lo.1976.21.1.0108

Burnham, K. P., & Anderson, D. R. (2004). Multimodel inference: Understanding AIC and BIC in model selection. *Sociological Methods and Research*. *33*(2), 261-304. https://doi.org/10.1177/0049124104268644

Burrage, D. M., & Garvine, R. W. (1988). Summertime hydrography at the shelfbreak front in the Middle Atlantic Bight. *Journal of Physical Oceanography*. *33*(2), 261–304. https://doi.org/10.1175/1520-0485(1988)018<1309:shatsf>2.0.co;2

Cai, W. J., Hu, X., Huang, W. J., Jiang, L. Q., Wang, Y., Peng, T. H., & Zhang, X. (2010). Alkalinity distribution in the western North Atlantic Ocean margins. *Journal of Geophysical Research*. *115*(C8), C08014. https://doi.org/10.1029/2009JC005482

Cai, W. J., Xu, Y. Y., Feely, R. A., Wanninkhof, R., Jönsson, B., Alin, S. R., et al. (2020). Controls on surface water carbonate chemistry along North American ocean margins. *Nature Communications*. *11*(1), 1–13. https://doi.org/10.1038/s41467-020-16530-z

Chapman, D. C., & Beardsley, R. C. (1989). On the origin of shelf water in the Middle Atlantic Bight. *Journal of Physical Oceanography*. *19*(3), 384–391. https://doi.org/10.1175/1520-0485(1989)019<0384:otoosw>2.0.co;2

Chen, C. T. A. (2002). Shelf-vs. dissolution-generated alkalinity above the chemical lysocline. *Deep-Sea Research Part II Topical Studies in Oceanography*, *49*(24–25), 5365–5375. https://doi.org/10.1016/S0967-0645(02)00196-0

Churchill, J. H., & Berger, T. J. (1998). Transport of Middle Atlantic Bight shelf water to the Gulf Stream near Cape Hatteras. *Journal of Geophysical Research*. *103*(C13), 30605–30621. https://doi.org/10.1029/98jc01628

Csanady, G. T., & Hamilton, P. (1988). Circulation of slopewater. *Continental Shelf Research*. *8*(5-7), 565–624. https://doi.org/10.1016/0278-4343(88)90068-4

Davis, C. V., Hewett, K., Hill, T. M., Largier, J. L., Gaylord, B., & Jahncke, J. (2018). Reconstructing aragonite saturation state based on an empirical relationship for northern California. *Estuaries and Coasts*, *41*, 2056–2069. https://doi.org/10.1007/s12237-018-0372-0

Dickson, A. G. (1990). Standard potential of the reaction: AgCl(s) + 1 2H2(g) = Ag(s) + HCl(aq), and the standard acidity constant of the ion HSO4- in synthetic sea water from 273.15 to 318.15 K. *The Journal of Chemical Thermodynamics*, *22*(2). 113–127. https://doi.org/10.1016/0021-9614(90)90074-Z

Dickson, A. G. (2010). The carbon dioxide system in seawater: Equilibrium chemistry and measurements. In U. Riebesell, V. J. Fabry L. Hansson & J. -P. Gattuso (Eds). *Guide to best practices for ocean acidification research and data reporting*, (pp. 17–40).

Dickson, A. G., Sabine, C. L., & Christian, J. R. (2007). *Guide to best practices for ocean CO_2 measurements*. PICES Special Publication.

Evans, W., Mathis, J. T., Winsor, P., Statscewich, H., & Whitledge, T. E. (2013). A regression modeling approach for studying carbonate system variability in the northern Gulf of Alaska. *Journal of Geophysical Research: Oceans*, *118*(1), 476–489. https://doi.org/10.1029/2012JC008246

Fennel, K. (2010). The role of continental shelves in nitrogen and carbon cycling: Northwestern North Atlantic case study. *Ocean Science*, *6*, 539–548. https://doi.org/10.5194/os-6-539-2010

Fennel, K., Wilkin, J., Previdi, M., & Najjar, R. (2008). Denitrification effects on air-sea CO_2 flux in the coastal ocean: Simulations for the northwest North Atlantic. *Geophysical Research Letters*, *35*(24), L24608. https://doi.org/10.1029/2008GL036147

Fourrier, M., Coppola, L., Claustre, H., D'Ortenzio, F., Sauzède, R., & Gattuso, J. P. (2020). A Regional neural network approach to estimate water-column nutrient concentrations and carbonate system variables in the Mediterranean Sea: CANYON-MED. *Frontiers in Marine Science*. *7*, 620. https://doi.org/10.3389/fmars.2020.00620

Gawarkiewicz, G. G., Todd, R. E., Plueddemann, A. J., Andres, M., & Manning, J. P. (2012). Direct Interaction between the Gulf Stream and the shelfbreak south of New England. *Scientific Reports*, *2*, 553. https://doi.org/10.1038/srep00553

Gledhill, D., White, M., Salisbury, J., Thomas, H., Mlsna, I., Liebman, M., Mook, B., et al. (2015). Ocean and coastal acidification off New England and Nova Scotia. *Oceanography*, *28*(2), 182. https://doi.org/10.5670/oceanog.2015.41

Gruber, N., Sarmiento, J. L., & Stocker, T. F. (1996). An improved method for detecting anthropogenic CO2in the oceans. *Global Biogeochemical Cycles*, *10*(4), 809–837. https://doi.org/10.1029/96gb01608

Goldman, J. C., & Brewer, P. G. (1980). Effect of nitrogen source and growth rate on phytoplankton-mediated changes in alkalinity1. *Limnology and Oceanography*, *25*(2), 352–357. https://doi.org/10.4319/lo.1980.25.2.0352

Hofmann, E. E., Cahill, B., Fennel, K., Friedrichs, M. A. M., Hyde, K., Lee, C., et al. (2011). Modeling the dynamics of continental shelf carbon. *Annual Review of Marine Science*. *3*, 93–122. https://doi.org/10.1146/annurev-marine-120709-142740

Houghton, R. W., Aikman, F., & Ou, H. W. (1988). Shelf-slope frontal structure and cross-shelf exchange at the New England shelf-break. *Continental Shelf Research*. *8*(5-7), 687–710. https://doi.org/10.1016/0278-4343(88)90072-6

Houghton, R. W., Hebert, D., & Prater, M. (2006). Circulation and mixing at the New England shelfbreak front: Results of purposeful tracer experiments. *Progress in Oceanography*. *70*(2-4), 289–312. https://doi.org/10.1016/j.pocean.2006.05.001

Jiang, L. Q., Carter, B. R., Feely, R. A., Lauvset, S. K., & Olsen, A. (2019). Surface ocean pH and buffer capacity: Past, present and future. *Scientific Reports*. *9*(1), 1–11. https://doi.org/10.1038/s41598-019-55039-4

Juranek, L. W., Feely, R. A., Gilbert, D., Freeland, H., & Miller, L. A. (2011). Real-time estimation of pH and aragonite saturation state from Argo profiling floats: Prospects for an autonomous carbon observing strategy. *Geophysical Research Letters*. *38*(17), L17603. https://doi.org/10.1029/2011GL048580

Juranek, L. W., Feely, R. A., Peterson, W. T., Alin, S. R., Hales, B., Lee, K., Sabine, C., et al. (2009). A novel method for determination of aragonite saturation state on the continental shelf of central Oregon using multi-parameter relationships with hydrographic data. *Geophysical Research Letters*, *36*(24), L24601. https://doi.org/10.1029/2009GL040778

Kim, T. W., Lee, K., Feely, R. A., Sabine, C. L., Chen, C. T. A., Jeong, H. J., & Kim, K. Y. (2010). Prediction of Sea of Japan (East Sea) acidification over the past 40 years using a multiparameter regression model. *Global Biogeochemical Cycles*, *24*(3). https://doi.org/10.1029/2009GB003637

Kutner, M., Nachtsheim, C., & Neter, J. (2004). *Applied linear regression models* (4th ed.). McGraw-Hill Irwin.

Langdon, C. (2011). Rosenstiel School of Marine and Atmospheric Science. *Temperature, salinity, nutrients, freons, oxygen, currents (ADCP), underway and other measurements collected in the Gulf of Mexico and Atlantic as part of the Gulf of Mexico and East Coast Carbon Cruise (GOMECC) 2007 (NCEI Accession 0066603)*. NOAA National Centers for Environmental Information. Dataset [indicate subset used] https://accession.nodc.noaa.gov/0066603

Laurent, A., Fennel, K., Cai, W. J., Huang, W., Barbero, L., & Wanninkhof, R. (2017). Eutrophication-induced acidification of coastal waters in the northern Gulf of Mexico: Insights into origin and processes from a coupled physical-biogeochemical model. *Geophysical Research Letters*, *44*, 946–956. https://doi.org/10.1002/2016GL071881

Lee, K., Tong, L. T., Millero, F. J., Sabine, C. L., Dickson, A. G., Goyet, C., et al. (2006). Global relationships of total alkalinity with salinity and temperature in surface waters of the world's oceans. *Geophysical Research Letters*, *33*, L19605. https://doi.org/10.1029/2006GL027207

Lee, K., Wanninkhof, R., Feely, R. A., Millero, F. J., & Peng, T. H. (2000). Global relationships of total inorganic carbon with temperature and nitrate in surface seawater. *Global Biogeochemical Cycles*, *14*(3), 979–994. https://doi.org/10.1029/1998GB001087

Linder, C. A., & Gawarkiewicz, G. (1998). A climatology of the shelfbreak front in the Middle Atlantic Bight. *Journal of Geophysical Research*. *103*(C9), 18405–18423. https://doi.org/10.1029/98JC01438

Li, B., Watanabe, Y. W., & Yamaguchi, A. (2016). Spatiotemporal distribution of seawater pH in the North Pacific subpolar region by using the parameterization technique. *Journal of Geophysical Research: Oceans*. *121*(5), 3435–3449. https://doi.org/10.1002/2015JC011615

Loder, J. W., Petrie, B., & Gawarkiewicz, G. (1998). The coastal ocean off northeastern North America: A large-scale view. *The Sea*. *11*, 105–138.

Lozier, M. S., & Gawarkiewicz, G. (2001). Cross-frontal exchange in the Middle Atlantic Bight as evidenced by surface drifters. *Journal of Physical Oceanography*. *31*(8), 2498–2510. https://doi.org/10.1175/1520-0485(2001)031<2498:cfeitm>2.0.co;2

Lueker, T. J., Dickson, A. G., & Keeling, C. D. (2000). Ocean pCO_2 calculated from dissolved inorganic carbon, alkalinity, and equations for K1 and K2: Validation based on laboratory measurements of CO_2 in gas and seawater at equilibrium. *Marine Chemistry*, *70*(3), 105–119. https://doi.org/10.1016/S0304-4203(00)00022-0

Martin, J. H., Knauer, G. A., Karl, D. M., & Broenkow, W. W. (1987). VERTEX: Carbon cycling in the northeast Pacific. *Deep-Sea Research Part A, Oceanographic Research Papers*, *34*(2), 267–285. https://doi.org/10.1016/0198-0149(87)90086-0

Millero, F. J., Lee, K., & Roche, M. (1998). Distribution of alkalinity in the surface waters of the major oceans. *Marine Chemistry*, *60*(2), 111–130. https://doi.org/10.1016/S0304-4203(97)00084-4

Orr, J. C., Epitalon, J. M., Dickson, A. G., & Gattuso, J. P. (2018). Routine uncertainty propagation for the marine carbon dioxide system. *Marine Chemistry*. *207*, 84–107. https://doi.org/10.1016/j.marchem.2018.10.006

Patsavas, M. C., Byrne, R. H., Wanninkhof, R., Feely, R. A., & Cai, W. J. (2015). Internal consistency of marine carbonate system measurements and assessments of aragonite saturation state: Insights from two U.S. coastal cruises. *Marine Chemistry*. *176*, 9–20. https://doi.org/10.1016/j.marchem.2015.06.022

Peng, T. H., & Broecker, W. S. (1987). C/P ratios in marine detritus. *Global Biogeochemical Cycles*, *1*(2), 155–161. https://doi.org/10.1029/GB001i002p00155

Pershing, A. J., Alexander, M. A., Hernandez, C. M., Kerr, L. A., Le Bris, A., Mills, K. E., Nye, J. A., et al. (2015). Slow Adaptation in the Face of Rapid Warming Leads to Collapse of the Gulf of Maine Cod Fishery. *Science*, *350*(6262), 809–812. https://doi.org/10.1126/science.aac9819

Pilcher, D. J., Naiman, D. M., Cross, J. N., Hermann, A. J., Siedlecki, S. A., Gibson, G. A., & Mathis, J. T. (2019). Modeled effect of coastal biogeochemical processes, climate variability, and ocean acidification on aragonite saturation sate in the Bering Sea. *Frontiers in Marine Science*, *5*, 508. https://doi.org/10.3389/fmars.2018.00508

Quinn, G. P., & Keough, M. J. (2002). *Experimental design and data analysis for biologists*, Cambridge: Cambridge University Press. https://doi.org/10.1017/cbo9780511806384

Ramp, S. R., Schlitz, R. J., & Wright, W. R. (1985). The deep flow through the Northeast Channel, Gulf of Maine. *Journal of Physical Oceanography*, *15*, 1790–1808. https://doi.org/10.1175/1520-0485(1985)015<1790:tdfttn>2.0.co;2

Redfield, A. C., Ketchum, B. H., & Richards, F. A. (1963). The influence of organisms on the composition of sea water. *The Sea*, *2*, 26–77.

Rheuban, J. E., Doney, S. C., McCorkle, D. C., & Jakuba, R. W. (2019). Quantifying the effects of nutrient enrichment and freshwater mixing on coastal ocean acidification. *Journal of Geophysical Research: Oceans*. *124*(12), 9085–9100. https://doi.org/10.1029/2019JC015556

Salisbury, J. E. (2017). Dissolved inorganic carbon, total alkalinity, pH, nutrients and other variables collected from profile and discrete sample observations using CTD, Niskin bottle, and other instruments from NOAA Ship Gordon. In *Gunter off the U.S. East coast during the East Coast ocean acidification (GU-15-04 ECOA1) from 2015-06-20 to 2015-07-23 (NCEI accession 0159428)*. NOAA National Centers for Environmental Information. Dataset. https://doi.org/10.7289/v5vt1q40

Salisbury, J. E., & Jönsson, B. F. (2018). Rapid warming and salinity changes in the Gulf of Maine alter surface ocean carbonate parameters and hide ocean acidification. *Biogeochemistry*, *141*, 401–418. https://doi.org/10.1007/s10533-018-0505-3

Salisbury, J. E., & Shellito, S. M. (2019). *Dissolved inorganic carbon, total alkalinity, pH, nutrients and other variables collected from discrete profile observations using CTD, Niskin bottle, and other instruments in the East Coast of the U.S. and Canada during the 2nd East Coast Ocean Acidification (ECOA2, or ECOA-2) cruise from 2018-06-25 to 2018-07-29 (NCEI Accession 0196419)*. NOAA National Centers for Environmental Information. Dataset. https://doi.org/10.25921/f4vg-g356

Salisbury, J., Vandemark, D., Hunt, C., Campbell, J., Jonsson, B., Mahadevan, A., McGillis, W., et al. (2009). Episodic riverine influence on surface DIC in the coastal Gulf of Maine. *Estuarine, Coastal and Shelf Science*, *80*(1), 108–118. https://doi.org/10.1016/j.ecss.2008.12.021

Sarmiento, J. L., & Gruber, N. (2006). *Ocean biogeochemical dynamics*. Princeton University Press. http://www.jstor.org/stable/j.ctt3fgxqx

Sauzède, R., Bittig, H. C., Claustre, H., Pasqueron de Fommervault, O., Gattuso, J.-P., Legendre, L., & Johnson, K. S. (2017). Estimates of Water-Column Nutrient Concentrations and Carbonate System Parameters in the Global Ocean: A Novel Approach Based on Neural Networks. *Frontiers in Marine Science*, *4*, https://doi.org/10.3389/fmars.2017.00128

Siedlecki, S. A., Kaplan, I. C., Hermann, A. J., Nguyen, T. T., Bond, N. A., Newton, J. A., et al. (2016). Experiments with seasonal forecasts of ocean conditions for the northern region of the California Current upwelling system. *Scientific Reports*, *6*(1), 1–18. https://doi.org/10.1038/srep27203

Siedlecki, S. A., Pilcher, D. J., Hermann, A. J., Coyle, K., & Mathis, J. (2017). The Importance of Freshwater to Spatial Variability of Aragonite Saturation State in the Gulf of Alaska. *Journal of Geophysical Research: Oceans*, *122*, 8482–8502. https://doi.org/10.1002/2017JC012791

Takahashi, T., Broecker, W. S., & Langer, S. (1985). Redfield Ratio Based on Chemical Data from Isopycnal Surfaces. *Journal of Geophysical Research*, *90*(C4), 6907–6924. https://doi.org/10.1029/JC090iC04p06907

Takeshita, Y., Johnson, K. S., Coletti, L. J., Jannasch, H. W., Walz, P. M., & Warren, J. K. (2020). Assessment of pH dependent errors in spectrophotometric pH measurements of seawater. *Marine Chemistry*, *223*, 103801. https://doi.org/10.1016/j.marchem.2020.103801

Thomas, H. (2002). Remineralization ratios of carbon, nutrients, and oxygen in the north Atlantic Ocean: A field databased assessment. *Global Biogeochemical Cycles*, *16*(3), 1051. https://doi.org/10.1029/2001GB001452

Townsend, D. W. (1991). Influences of oceanographic processes on the biological productivity of the Gulf of Maine. *Reviews in Aquatic Sciences*, *5*(3–4), 211–230.

Townsend, D. W. (1998). Sources and cycling of nitrogen in the Gulf of Maine. *Journal of Marine Systems*. *16*(3-4), 283–295. https://doi.org/10.1016/S0924-7963(97)00024-9

Townsend, D. W., Thomas, A. C., Mayer, L. M., Thomas, M., & Quinlan, J. (2004). Oceanography of the northwest Atlantic continental shelf. In A. R. Robinson, & K. Brink (Eds.), *In the Sea: The global coastal ocean: Interdisciplinary regional Studies and syntheses* Vol. 14A. Cambridge, MA: Harvard University Press.

van Heuven, S., Pierrot, D., Rae, J. W. B., Lewis, E., & Wallace, D. W. R. (2011). *MATLAB program developed for CO_2 system calculations. ORNL/CDIAC-105b. ORNL/CDIAC-105b. Carbon dioxide information analysis center*. Oak Ridge, TN: Oak Ridge National Laboratory, U.S. Department of Energy. https://doi.org/10.3334/CDIAC/otg.CO2SYS_MATLAB_v1.1

Wallace, R. B., Baumann, H., Grear, J. S., Aller, R. C., & Gobler, C. J. (2014). Coastal ocean acidification: The other eutrophication problem. *Estuarine, Coastal and Shelf Science*, *148*(1–13). https://doi.org/10.1016/j.ecss.2014.05.027

Wang, Z. A., Lawson, G. L., Pilskaln, C. H., & Maas, A. E. (2017). Seasonal controls of aragonite saturation states in the Gulf of Maine. *Journal of Geophysical Research: Oceans*, *122*(1), 372–389. https://doi.org/10.1002/2016JC012373

Wang, Z. A., Lawson, G. L., Pilskaln, C. H., & Maas, A. E. (2018). *Discrete profile measurements of dissolved inorganic carbon, total alkalinity, dissolved oxygen, temperature and salinity during the R/V Tioga ten cruises in Wilkinson Basin of the Gulf of Maine from 2013-05-21 to 2015-02-15 (NCEI Accession 0172591)*. NOAA National Centers for Environmental Information. Dataset. https://doi.org/10.7289/v5765cn9

Wang, Z. A., Wanninkhof, R., Cai, W. J., Byrne, R. H., Hu, X., Peng, T. H., & Huang, W. J. (2013). The Marine inorganic carbon system along the Gulf of Mexico and Atlantic coasts of the United States: Insights from a transregional coastal carbon study. *Limnology & Oceanography*, *58*(1), 325–342. https://doi.org/10.4319/lo.2013.58.1.0325

Wanninkhof, R., Barbero, L., Baringer, M. O., Byrne, R. H., Cai, W., Langdon, C., et al. (2014). Dissolved inorganic carbon, total alkalinity, pH, fugacity of carbon dioxide, and other variables from surface observations using Niskin bottle, flow through pump and other instruments from NOAA Ship Ronald H. In *Brown in the Gulf of Mexico and East coast of the United States during the second Gulf of Mexico and East coast carbon (GOMECC-2) cruise from 2012-07-22 to 2012-08-13 (NCEI accession 0117971)*. NOAA National Centers for Environmental Information. Dataset. https://doi.org/10.7289/v5542kj0

Wanninkhof, R., Barbero, L., Byrne, R., Cai, W. J., Huang, W., Zhang, W., Baringer, M., et al. (2015). Ocean acidification along the Gulf Coast and East Coast of the USA. *Continental Shelf Research*, *98*, 54–71. https://doi.org/10.1016/j.csr.2015.02.008

Weiss, R. F. (1970). The solubility of nitrogen, oxygen and argon in water and seawater. *Deep-Sea Research and Oceanographic Abstracts*, *17*(4), 721–735. https://doi.org/10.1016/0011-7471(70)90037-9

Xu, Y. Y., Cai, W. J., Wanninkhof, R., Salisbury, J., Reimer, J., & Chen, B. (2020). Long-term changes of carbonate chemistry variables along the north American East Coast. *Journal of Geophysical Research: Oceans. 125*(7), e2019JC015982. https://doi.org/10.1029/2019JC015982

Erratum

In the originally published version of this article, the images for Figures 5, 6, and 7 were incorrectly transposed due to a typesetting error. The error has been corrected, and this may be considered the official version of record.